Advanced Materials Technologies

ADVANCED MATERIALS TECHNOLOGIES
www.advmattechnol.com

RESEARCH ARTICLE

Liquid Metal is a Bulk Conductor

Monica Li[1] | Stephanie Woodman[1] | Dylan Shah[2] | Rebecca Kramer-Bottiglio[1]

[1]School of Engineering & Applied Science, Yale University, New Haven, Connecticut, USA | [2]Arieca, Inc., Pittsburgh, Pennsylvania, USA

Correspondence: Rebecca Kramer-Bottiglio (rebecca.kramer@yale.edu)

Received: 15 January 2026 | **Accepted:** 9 February 2026

Keywords: eutectic gallium-indium | liquid metal | soft robotics | stretchable electronics

ABSTRACT

As stretchable electronics enable fully soft robots and more comfortable wearables that conform to the human body, researchers have engineered a plethora of stretchable conductors. Inconsistencies in experimental techniques plague many of these candidate materials, leading to contradictory claims between similar studies. For example, the room-temperature liquid metal eutectic gallium-indium (EGaIn) has been reported to have a variety of electromechanical responses, ranging from strain insensitivity to strain sensitivity even greater than that of an incompressible bulk conductor. In this work, we seek to provide a unified theory for the electromechanical response of EGaIn. Specifically, we provide analytical and experimental results supporting the hypothesis that liquid metal is a bulk conductor. The key insight is that parasitic resistance—arising from contact points and unstrained regions—masks true material behavior, leading to apparent discrepancies across studies and falsely suppressed strain responses. Linear normalization can remove these differences and collapse a wide range of previously published data into a common curve, which matches bulk-conductor theory. Our experimental results, spanning various trace geometries, also match bulk conductor theory. We hope that this work resolves the debate on whether liquid metal is a bulk conductor while providing a framework to evaluate other stretchable conductors.

1 | Introduction

Stretchable electronics have applications to wearable devices, [1–4] soft robotics [5, 6], and more. [7] Many of the reported advances rely on stretchable interconnects made from eutectic gallium-indium (EGaIn), commonly referred to as liquid metal [8, 9]. Liquid metal interconnects can deform and flow to maintain conductivity during stretch. Researchers have also processed liquid metal into pastes and other composites to attain more desirable mechanical and magnetic properties, along with heightened electrical and thermal conductivities. [10, 11] Through various fabrication processes and amalgams, researchers utilize liquid metal for conductive traces in electronic circuits that are soft and highly stretchable [12–16]. Understanding the electrical resistance when undergoing deformations is critical to designing systems that are predictable, energetically efficient, and reliable over long periods of use. However, as discussed in our recent review "Are liquid metals bulk conductors?" [17] there are a wide range of reported strain responses, spanning sensitivities both above [18] below, [3, 17, 19–25], and agreeing with [14, 26] that of a bulk conductor. Our question was thus left unanswered, arguably raising more uncertainties than answers.

The bulk conductor model of a circuit element, known as Pouillet's Law, adequately describes the resistance of many metals. [27] This idealized model assumes a homogeneous and isotropic material with a uniform cross-section throughout the trace. If we assume the material is incompressible, we can rearrange the bulk conductor equation to have resistance in terms of strain, and use this model as the benchmark to compare stretchable conductors. If the material exhibits a strain response that matches that of a bulk conductor, then we consider the material a bulk conductor. If resistance changes very little with strain, we deem the material "strain insensitive." In much of the literature, materials exhibit

a strain response lower than that of a bulk conductor, but still increasing with strain; these we deem to have a suppressed strain response.

One explanation for suppressed electromechanical curves in liquid metal composites is the presence of tortuous conduction pathways [28]; however, this does not account for why even pure liquid metal traces can exhibit resistance lower than predicted by Pouillet's law.[17, 19] In our previous work [17], we demonstrated that differences in measurement techniques alone can lead to conflicting conclusions about the same material due to parasitic resistances in the experimental setups. Building on this, Monnens et al. proposed two primary mechanisms for suppressed strain response: contact resistance and the sintering and re-oxidation of liquid metal [29]. While contact resistance can be reduced—though not fully eliminated—with a four-point probe, the remaining hypotheses and supporting evidence do not sufficiently explain why encapsulated EGaIn and other stretchable conductors often deviate from bulk conductor behavior.

In this study, we resolve the inconsistencies shrouding the experimental and theoretical literature on the electromechanical response of liquid metal. First, we propose a model that accounts for all parasitic resistance with a single constant and a linear normalization that removes constant offsets (including the parasitic resistance) from the analysis. Then, we compile results from 12 previous studies, finding that this linear normalization indeed aligns the reported results remarkably well. Finally, we use linear normalization to evaluate a comprehensive set of experiments with liquid metal traces of varying geometry, both static and straining.

Collectively, we show that liquid metal, specifically neat EGaIn, behaves as a bulk conductor. Deviations from Pouillet-type behavior primarily result from parasitic resistances, either from the measurement setup (as we previously reported [17]) or from the sample itself (modeled here). This work provides a framework to disentangle experimental error from the strain behavior of novel formulations of liquid metal composites. That is, by establishing the baseline behavior of bulk liquid metal, we aim to clarify prior conflicting reports and enable future work to focus on effects such as oxidation, material additives, or polymer integration that genuinely impact performance. Additionally, this framework can be directly applied to evaluate other stretchable conductors for bulk-conductor behavior. By enabling more accurate characterization, it empowers designers of soft robots and wearable electronics to better predict system performance and select suitable components.

2 | Results

2.1 | Pouillet's Law

Pouillet's law describes the resistance of a homogeneous and isotropic material, with uniform cross-section throughout the trace [27]. This idealized model is appropriate for many resistors and conductors, and appears to be the go-to model across disciplines. The assumptions lead to a simple equation for electrical resistance:

$$R = \rho \frac{L}{A} \tag{1}$$

with the material resistivity ρ, trace length L, and cross-sectional area A. Longer traces have higher resistance, while larger cross-sectional areas have lower resistance. Note that conductivity is the inverse of resistivity, $\sigma = 1/\rho$.

Pouillet's law is easily extended to the conventional format with resistance in terms of strain, which is utilized in stretchable electronics research [14, 17, 26, 28]. Strain is defined as $\varepsilon = \Delta L/L_0$, for initial length L_0 and change in length ΔL. Assuming incompressibility and dividing by initial resistance R_0, we obtain (derivation in Supporting Information):

$$\frac{R}{R_0} = (1+\varepsilon)^2 \tag{2}$$

Thus, we have a candidate criterion for determining whether a material is a bulk conductor: if and only if its resistance follows Pouillet's Law. Otherwise, materials with negligible resistance change are "strain insensitive," while a strain response between strain insensitive and bulk conductor is referred to as a suppressed strain response. Although Pouillet's law is a purely geometric relation valid in both compression and tension, stretchable conductors are typically thin structures that do not experience uniform axial compression in practice. Accordingly, prior studies evaluate electrical behavior under tensile loading, and we likewise focus on uniaxial tension.

As a bulk conductor model, Pouillet's Law makes several simplifying assumptions. For example, the model does not account for the parasitic resistance of the measurement setup, which we previously found to be significant unless a four-point probe technique is used [17]. Additionally, the bulk conductor model does not consider unstrained portions of the circuit or the interfacial resistance between the liquid metal trace and connected components such as resistors or capacitors. In practice, eliminating all sources of parasitic resistance is nearly impossible. In our prior study [17], we subtracted an estimated parasitic resistance from the total measured resistance but still observed a suppressed strain response, indicating the presence of additional unaccounted sources. We also note that the oxide layer on the surface of the liquid metal traces is four orders of magnitude thinner than the smallest trace dimension [30], and therefore its contribution is assumed to be negligible. Taken together, these considerations suggest the need for a modified criterion to determine whether a conductor follows Pouillet's Law and exhibits bulk conductor behavior under experimental conditions.

2.2 | Parasitic Resistance in Liquid Metal Traces

Experimental error often presents itself as an increase in the total measured resistance. As our objective is to determine the intrinsic behavior of liquid metal, we are only interested in measuring the resistance of the straining part of the sample. Therefore, we consider the resistance contribution from all other parts of the circuit to be parasitic, including the unstrained liquid metal, material interfaces, copper wire, and measurement device

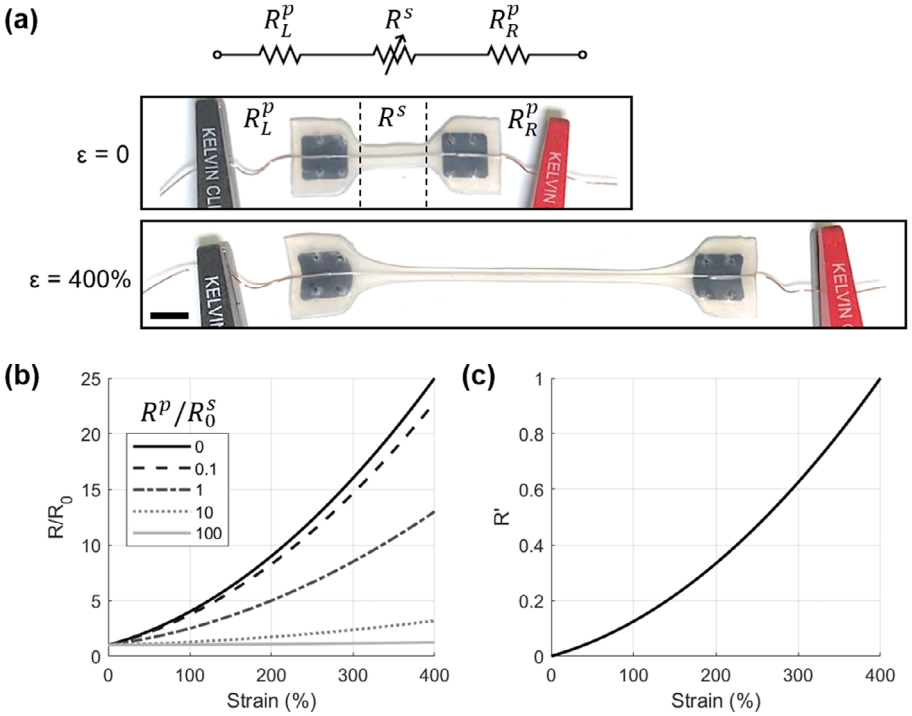

FIGURE 1 | Theoretical resistance of straining bulk conductor samples. (a) Resistor network for a liquid metal sample (top), along with an experimental sample that was at rest (middle) and strained to 400% (bottom). The measured resistance is the sum of the strained R^s and the parasitic resistances R^p, where the subscripts denote left and right side ($R^p = R_L^p + R_R^p$). Scale bar, 10 mm. (b) Relative resistance versus strain for theoretical bulk conductors with parasitic resistance R^p/R_0^s. (c) Linear normalization versus strain for the same bulk conductor and parasitic resistances shown in (b). Here, the curves perfectly collapse into one.

(Figure 1a). Albeit small (typically less than 1 Ω), the parasitic resistance may be significant compared to the sample resistance. We assume parasitic resistance is constant, and decompose the measured resistance R^m into the resistance of the straining portion of liquid metal R^s and the parasitic resistance R^p, such that the relative resistance is:

$$\frac{R^m}{R_0^m} = \frac{R^s + R^p}{R_0^s + R^p} \tag{3}$$

The measured relative resistance exhibits vastly different behavior depending on the ratio between R^p to R_0^s (Figure 1b). Even if the straining resistance R^s is that of a bulk conductor, the addition of parasitic resistance gives the appearance of a suppressed strain response.

Seeking to extend our model to explain the full range of results reported in the literature, we explored using linear normalization (also known as min–max or feature normalization) to analyze strain sensitivity. Linear normalization subtracts the minimum value and divides by the range, scaling the dataset between zero and one [31]:

$$R'_m = \frac{R^m - R_0^m}{R_{max}^m - R_0^m} \tag{4}$$

R_{max}^m denotes the measured resistance at maximum strain, with R_0^m the measured resistance at zero strain. This normalization removes the parasitic resistance without explicitly calculating its value, as the parasitic resistance terms cancel out. Linear normalization offers advantages over previous analysis methods, particularly when it is unclear how much of the measured resistance change is due to straining conductive material versus parasitic contributions. The change in measured resistance is the same as the change in straining resistance:

$$R^m - R_0^m = (R^s + R^p) - (R_0^s + R^p) = R^s - R_0^s \tag{5}$$

Using Equation (1), we present the idealized, or theoretical, linear normalization curve for a bulk conductor in terms of strain (derived in the Supporting Information):

$$R'_\varepsilon = \frac{\varepsilon(\varepsilon + 2)}{\varepsilon_{max}(\varepsilon_{max} + 2)} \tag{6}$$

Thus, any bulk conductor that is measured in series with a parasitic resistance should follow a single curve, where $R'_m = R'_\varepsilon$ (Equations (4) and (6)). Indeed, linear normalization collapses all the varied relative parasitic resistances from Figure 1b onto a single bulk conductor line in Figure 1c.

Linear normalization pins the ends to zero and one, so to evaluate goodness-of-fit for the model, we need to compare the curve shape rather than absolute values. To quantify how closely the data matches that of a bulk conductor, we define the residual as the difference between the measured linear normalization R'_m and that predicted based on strain R'_ε:

$$\text{Residual} \equiv R'_m - R'_\varepsilon = \frac{R^m - R_0^m}{R_{max}^m - R_0^m} - \frac{\varepsilon(\varepsilon + 2)}{\varepsilon_{max}(\varepsilon_{max} + 2)} \tag{7}$$

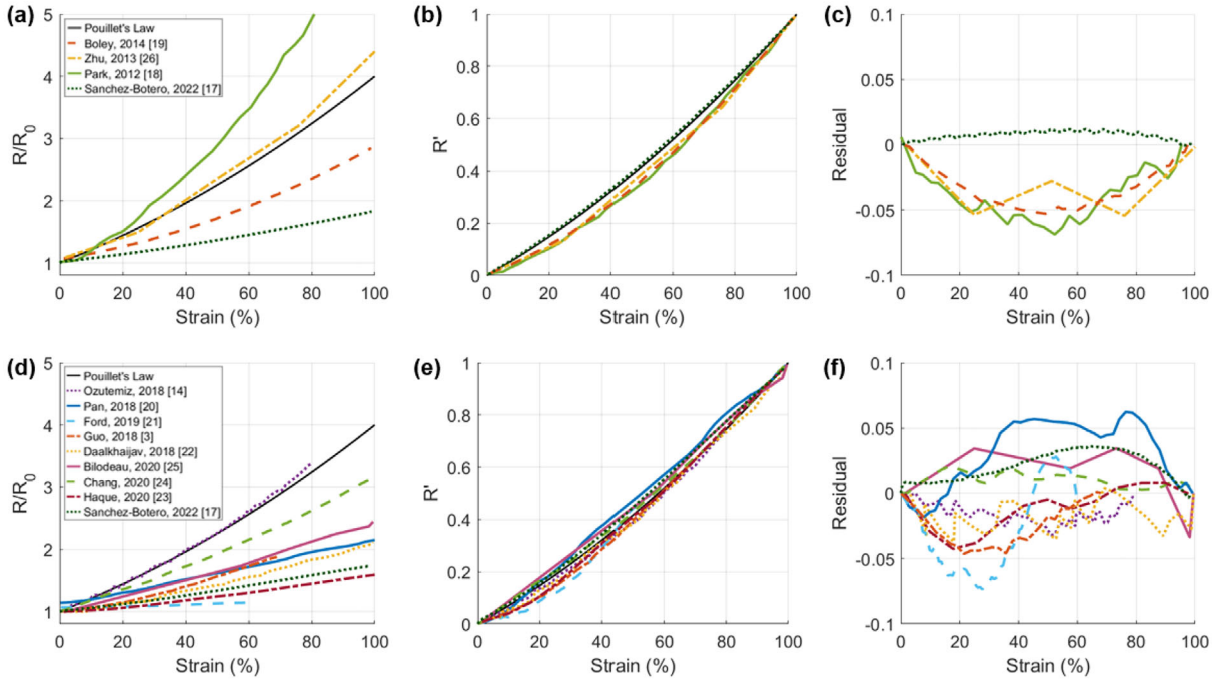

FIGURE 2 | Previously reported electromechanical responses of liquid metal conductors, shown using (a) traditional R/R_0 non-dimensionalization and (b) linear normalization. Panel (c) shows the residual between the linear normalization and the bulk conductor model for neat EGaIn. The analogous analyses for EGaIn composites are given in (d), (e), and (f), respectively. Theoretical bulk conductor behavior is plotted as a solid black line in (a, b, d, e) and would be a flat horizontal line at zero in (c, f).

The residual compares the strain response to that of a bulk conductor, which follows an approximately quadratic relationship. A positive residual indicates a more linear response, while a negative residual suggests higher-order conductivity behavior relative to the bulk conductor curve. Generally, if the residual stays small across all measured strains, then a bulk conductor curve is a good match for the data. An expansion to non-uniform cross-sections of conductive traces is presented in the Supporting Information.

Building upon the previous analysis, we hypothesized that experimental data that appear to have a suppressed strain response relative to the conventional R/R_0 non-dimensionalization (Equation (2)) may still be a bulk conductor and thus match the bulk conductor curve when parasitic resistance is removed using the linear normalization metric (Equation (4); Figure 2). We therefore re-examined several EGaIn [17–19, 26] and EGaIn composite [3, 14, 17, 20–24] datasets using 1) relative resistance (Equation (2) and Figure 2a,d) and 2) linear normalization (Equation (4), Figure 2b,e) with residuals (Equation (7) and Figure 2c,f).

The neat EGaIn data have varied strain responses when presented as relative resistance (Figure 2a). Analogous to theoretical resistance (Figure 1b), we hypothesize that liquid metal is a bulk conductor and that the wide spread of strain responses observed in relative resistance is due to parasitic resistance in the measurement. When plotted using linear normalization (Figure 2b), the data and bulk conductor curve seemingly collapse onto each other, as seen in the theory (Figure 1c). Three of the prior results [18, 19, 26] visually have similarly negative residuals (Figure 2c), indicating either that cubic or higher-order terms may be involved in the specimens' response (driven by mechanisms we do not hypothesize here, or measurement artifacts). The results from Sanchez et al. [17] have a positive residual with a magnitude of approximately one percent. The experimental error is not provided in many of these results, so the apparent residual may be an artifact of noise. Thus, the conductive behavior of these materials is still uncertain. The EGaIn composite data are similar, where varied strain responses in relative resistance (Figure 2d) collapse onto the bulk conductor curve in linear normalization (Figure 2e). The residuals of the composites have varied shapes, all with magnitudes below 7% (Figure 2f). The residual magnitude alone is insufficient to draw conclusions about the conductivity of these materials; additional information about the experimental setup and measurement uncertainty is required.

The shape of the bulk conductor curve depends on the maximum strain, which is pertinent because we evaluate the results in linear normalization based on curve shape (Figure 2, Figure S9, Figure S10). At small strains (≤~100%), a material exhibiting a linearly increasing strain response could be mistaken for a bulk conductor (Figure S9). For materials that cannot be stretched further, alternative methods—outlined in the Supporting Information—should be used to determine bulk conductivity more reliably. For the prior strain responses that were reported beyond 100% strain, [20, 22, 23, 26] we plotted the results as linear normalization and residual, finding a subset of results to clearly deviate from bulk conductor theory (Figure S10). If the data does not match the bulk conductor curve, the material could still be a bulk conductor. We cannot rule out that the experimental setup is erroneous or that one of our assumptions is invalid.

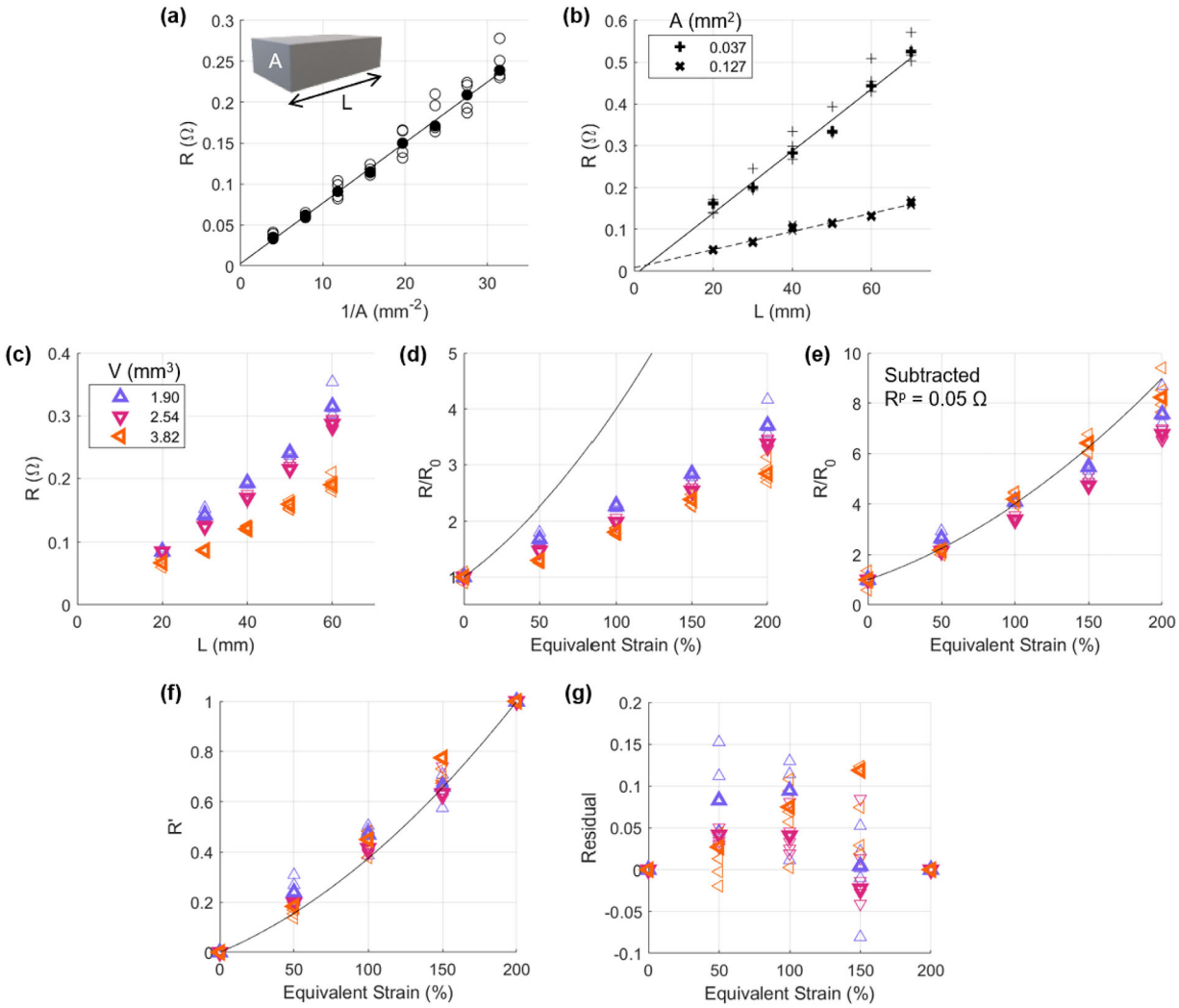

FIGURE 3 | Resistance measurements of static (unstrained) liquid metal samples. We present all measurements, with the median measurement in bold (N=5). (a) Varied cross-sectional area with constant length (L=30 mm). The inset shows a trace schematic with length L and area A, where current runs parallel to the length. (b) Varied length with two constant cross-sectional areas (A=0.037, 0.127 mm^2). In (a) and (b), we additionally plot the linear regression that minimizes the sum of squared error. (c) The resistance of unstrained samples with three trace volumes for lengths ranging from 20 to 60 mm. The cross-sectional area was selected to achieve approximately the prescribed volume at each length (V = L × A), thereby simulating the strained geometry without mechanically stretching the sample. The data from (c) are replotted as (d) relative resistance versus equivalent strain, (e) relative resistance versus equivalent strain after subtracting the estimated parasitic resistance ($R^p = 0.05\ \Omega$), along with (f) linear normalization and (g) the corresponding residual.

2.3 | Static Trace Geometry

We postulated that the stretching action could conflate underlying material properties and aimed to evaluate bulk conductivity based on the non-modified form of Pouillet's Law, $R = \rho\frac{L}{A}$ (Equation (1)). Thus, we experimentally tested liquid metal traces of varying length and cross-sectional area to achieve the geometry that would be attained if the sample were strained to that prescribed length, a process we define as the sample being under "equivalent strain" (Figure S12a). Equivalent strain refers to varying the trace geometry to simulate the straining of liquid metal while using an unstrained sample.

The liquid metal was encapsulated by a silicone elastomer and connected to the four-point probe measurement device using copper wire. We first varied the cross-sectional area while keeping the trace length constant. We plotted resistance against the inverse of area, since Pouillet's Law predicts this relationship to be linear, thereby aiding in the visualization of goodness-of-fit (Figure 3a). Then, we tested traces of various lengths with two cross-sectional areas (Figure 3b). The results from both sets of experiments, independently varying length and area, support that liquid metal is a bulk conductor (Table 1).

We fabricated samples with varying lengths and cross-sectional areas, such that the unstretched geometries simulated trace dimensions under strain. Three different trace volumes ($V = L \times A$) were tested, corresponding to equivalent strain values ranging from 0% to 200% in 50% increments. This approach was designed to decouple the effects of trace geometry from unknown material

TABLE 1 | Tabulated values of static liquid metal samples corresponding to Figure 3a,b: resistivity ρ, parasitic resistance R^p, and R-squared value of the linear fit R^2. Parasitic resistance is calculated based on the transmission line model [32]. The negative parasitic resistance is attributed to experimental error. In comparison, the previously reported resistivity value is 2.94×10^{-4} Ω · mm and was also calculated using Equation (1). [33]

	ρ ($\times10^{-4}$ Ω · mm)	R^p (Ω)	R^2
Area sweep, L=30 mm (Figure 3a)	2.46	0.003	0.997
Length sweep, A=0.037 mm^2 (Figure 3b)	2.70	−0.010	0.983
Length sweep, A=0.127 mm^2 (Figure 3b)	2.76	0.008	0.982

behaviors that may arise when liquid metal is stretched. We present the raw resistance values plotted against trace volumes V = {1.90, 2.54, 3.82} mm^3 (Figure 3c). A base trace length of L_0 = 20 mm corresponds to cross-sectional areas A_0 = {0.095, 0.127, 0.191} mm^2. To simulate strained geometries, we increased the trace length while decreasing the cross-sectional area, keeping the volume constant. The resulting relative resistance R/R_0 exhibits a suppressed strain response compared to that of an ideal bulk conductor (black line in Figure 3d). We note that samples with smaller cross-sectional areas (and correspondingly larger lengths) exhibit increased scatter, which we attribute to slight overfilling of the trace geometry that introduces local nonuniformities.

When an estimated parasitic resistance of 0.05 Ω, attributed to copper contacts and wire leads, is subtracted from all traces, the data align more closely with the expected behavior of a bulk conductor (Figure 3e). However, some deviations remain. Introducing sample-specific parasitic resistance values would collapse the data onto the bulk conductor curve; however, here we intentionally apply a single correction to evaluate the model without overfitting.

To assess bulk conductor behavior without subtracting an estimated parasitic resistance, we plot the data using linear normalization (R') and the corresponding residuals (Figure 3f,g). While the general electromechanical behavior is clearly captured, the residuals are higher than our other experiments, with one set of traces (volume 3.82 mm^3) exhibiting a median residual exceeding 10%.

2.4 | Resistance and Strain

The previous set of static experiments excluded factors introduced when a sample is under strain, including dynamic stretching or strain-dependent resistivity. To test the dynamic behavior of EGaIn, we measured the resistance of straining liquid metal traces and analyzed the data using the linear normalization metric. First, we compared the strain-resistance response of liquid metal to that of a known bulk conductor and a known strain-insensitive sample. Second, we tested liquid metal with varying cross-sectional area A and aspect ratio H/W. Third, we estimated the parasitic resistance by varying trace length L (also known as the transmission line method [32]). These experiments independently test the influence of conductor material composition, trace geometry, and the contact resistance of our measurement setup, respectively.

We tested liquid metal in comparison to positive and negative controls: a known bulk conductor and strain-insensitive geometry (Figure 4). Our positive control was neat gallium, a pure element we expect to be a bulk conductor. [34, 35] Using encapsulated pure gallium further reduces uncertainties related to potential phase separation, solid inclusions, or oxidation that may be present in GaIn alloys such as EGaIn. We fabricated traces of two different cross-sections (A = 0.076 and 0.152 mm^2, Figure S12b) for liquid metal and neat gallium, with L_0 = 17 mm. Serpentine copper wire was our negative control (Figure S13). Although copper is a bulk conductor, we expected the resistance to stay constant under strain due to the serpentine geometry. As the sample stretched, the serpentine pattern unwound, keeping the trace length and cross-sectional area constant. At strains as high as 100%, the serpentine copper samples exhibited a strain-insensitive response (Figure 4a), while liquid metal and gallium appeared to have a suppressed strain response when plotted as relative resistance (Figure 4b). Linear normalization showed that both materials are bulk conductors (Figure 4c), with a featureless residual curve (Figure 4d). We define a featureless residual as one that is visually flat and where zero is within one standard deviation (shaded region) across all strains.

We then fabricated traces with varying cross-sectional areas while holding the aspect ratio constant, and vice versa, then stretched the traces to 400% strain (Figure 5). We observed that traces with larger cross-sectional areas had lower resistance (Figure 5a). The traces with larger areas exhibited a more suppressed strain response, due to the relatively higher parasitic resistance (Figure 5b). Using linear normalization, the data for all cross-sections closely match the bulk conductor curve (Figure 5c), as affirmed by the featureless residual (Figure 5d). We similarly observed bulk conductor behavior in traces with varying aspect ratios (Figure 5e–h). Pouillet's Law is ambivalent to aspect ratio, so it is not surprising that aspect ratio did not substantially affect the electromechanical behavior.

To isolate the starting trace length parameter, we strained liquid metal traces with the gauge length L_0 = 3.5, 17.5, 31.5 mm (A = 0.127 mm^2, Figure S12c) up to 300% strain. The longer traces had a higher total resistance (Figure 6a), which is consistent with Pouillet's Law. We similarly observed the appearance of a suppressed strain response when analyzed using relative resistance, with higher suppression in the shorter traces (Figure 6b). Linear normalization removes parasitic resistance from the analysis and shows that all our traces behaved as bulk conductors (Figure 6c), with low to moderate residuals (staying below ~0.1, Figure 6d). We estimated the parasitic resistance from the unstrained samples using the transmission line model to be R^p = 0.052 Ω (Figure 6e). Finally, we replotted the relative resistance after subtracting parasitic resistance (Figure 6f). The resultant data was closer to the bulk conductor curve but still exhibited a slightly

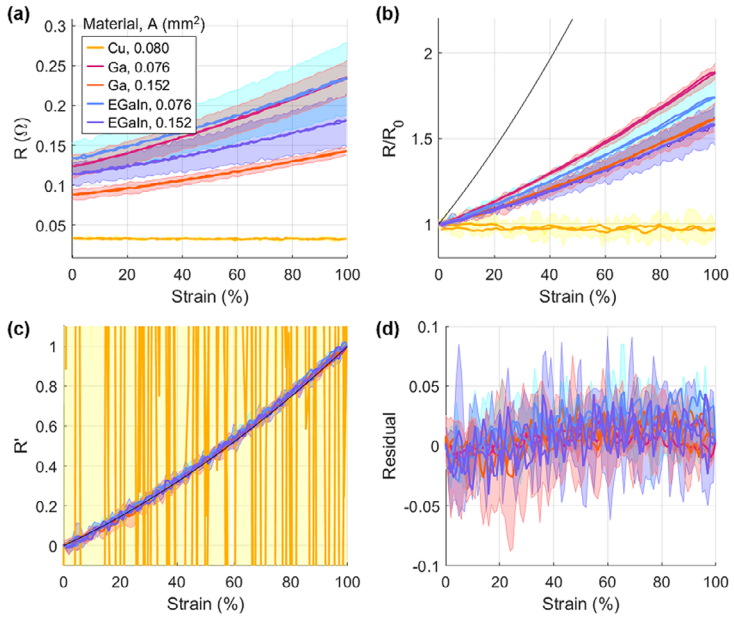

FIGURE 4 | Electromechanical behavior of EGaIn, gallium, and serpentine copper (N=5). Plotted with strain, (a) resistance responses, (b) relative resistance, (c) normalized resistance, and (d) residual of the normalized resistance and bulk conductor theory. We compare the measured resistances to Pouillet's Law, shown in (b) and (c) as the solid black line. We omit the copper measurements in (d) because the R' curve is noisy, as shown in (c).

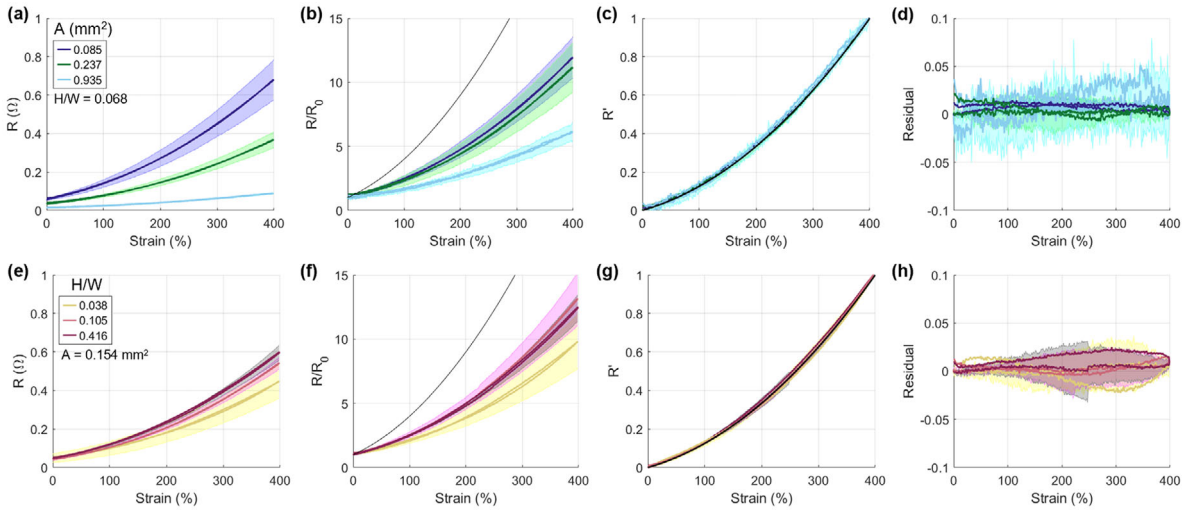

FIGURE 5 | Strain response for traces with varying cross-sectional area and aspect ratio (N=4), plotted as (a) measured resistance, (b) relative resistance, (c) linearly normalized resistance, and (d) residual. The dataset for A=0.085 mm^2 only has three samples (N=3). The analogous plots for varying aspect ratio are shown in (e–h).

suppressed response. As such, future researchers could subtract the calculated parasitic resistance and report $(R - R_0)/R_0$, but might not obtain the accurate material strain response. We suggest utilizing linear normalization and evaluating the residual as the bulk conductor determination tool.

The experimental results herein show that liquid metal is a bulk conductor. Specifically, the data are consistent with Pouillet's Law in the original form (Equation (1)) and its modification to linear normalization (combining Equations (4) and (6)), while parasitic resistance gives an erroneous appearance of suppressed strain response when analyzed as relative resistance (Equation (2)).

3 | Conclusion

We conclude that liquid metal, namely neat EGaIn, is a bulk conductor. Experimentally isolating the resistance of straining liquid metal is difficult, as non-straining circuit components and the measurement device can contribute to parasitic resistance. Parasitic resistance produced the appearance of a suppressed strain response when using relative resistance analysis (R/R_0). Using linear normalization to analytically remove the effect of parasitic resistance, we unveiled the underlying conductive nature of straining liquid metal.

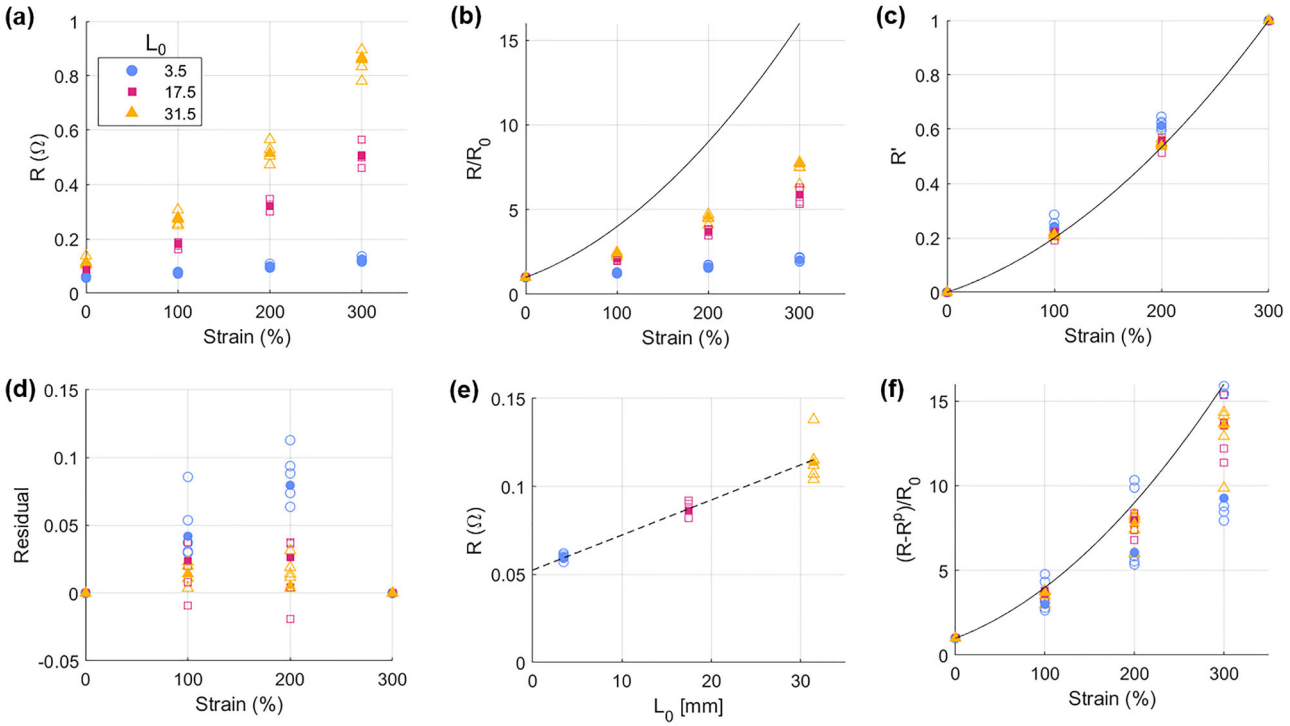

FIGURE 6 | Strained traces with varied sample length, L_0={3.5, 17.5, 31.5} mm and area, A=0.127 mm^2. We show each datapoint as an open circle and the median value as a filled-in circle. We plot (a) resistance, (b) relative resistance, (c) linear normalization, and (d) residual versus strain. In (e), we plotted unstrained resistance versus sample length, where the vertical axis intercept is parasitic resistance, R^p=0.052 Ω (R^2=1.0). We subtract R^p from the data and replot (b) in (f).

We began by comparing the resistance of static traces to predictions from the original Pouillet's Law. Next, we measured the resistance of EGaIn traces under strain, using melted gallium and serpentine copper wire as positive and negative controls, respectively. We also tested traces with varied geometries (cross-sectional area, aspect ratio, and length) stretched up to 400% strain. Across all experiments, the liquid metal traces consistently exhibited bulk conductor behavior, confirming that neat EGaIn functions as a bulk conductor under strain.

Based on these results, we recommend several best practices to assess the conductivity of a stretchable material. First, the resistance of traces with varying lengths and cross-sectional areas should be measured under no strain, so the conductivity of a material is evaluated solely based on Pouillet's Law. Then, the material should be measured under strain, where a single trace geometry is sufficient. We recommend straining samples to the highest possible elastic strain (>100%) to reduce the chance of falsely deeming the material a bulk conductor, due to apparent linearity when the strain range is small. Further, the use of min–max linear normalization enables analysis of the strain response with parasitic resistance removed. A featureless residual indicates that (1) the material is a bulk conductor and (2) our assumptions hold, which include material incompressibility, strain-independent parasitic resistance, and accurately reported strain. Greater accuracy in strain reporting could be attained using visual strain measurement techniques. [36] If the residual has a shape with significant magnitude, either the material is not a bulk conductor or our assumptions are invalid, and testing additional trace geometries may provide insight into the materials' likeness to bulk conductivity. Presenting the raw data alongside linear normalization can improve transparency, while unveiling the intrinsic behavior of the conductor.

Liquid metal is increasingly used in stretchable circuits that transmit both power and analog signals in wearable electronics and soft robotics. Because circuit resistance as a function of strain influences both power delivery and signal fidelity, it serves as a figure of merit in the development of stretchable electronics. Understanding the electromechanical properties of the trace material is therefore essential.

To enhance manufacturability and circuit durability, liquid metal is often combined with solid particles to form composites with improved mechanical robustness. The addition of fillers (including oxides, particles, or polymer matrices) in liquid metal composites can introduce mechanisms (such as microstructural rearrangement, inhomogeneous oxide distribution, or percolation) that lead to deviations from bulk conductor behavior under strain. Understanding these effects is an important direction for future work. It is also important to distinguish between deviations from bulk conductor behavior that arise from intrinsic material mechanisms and those that result from experimental or analytical artifacts such as parasitic resistance, contact effects, or normalization choices. The framework presented here is intended to isolate the latter, providing a consistent baseline for identifying and interpreting genuinely material-driven departures from bulk conduction in liquid metal-based systems.

We hope that the data processing method presented herein will be utilized to evaluate the electromechanical behavior of stretchable conductors for various use cases, ranging from sensors to power

traces to resistance-insensitive digital components. A deeper understanding of conductivity in these systems will support the reliable integration of stretchable circuits into everyday technologies.

4 | Materials and Methods

The material preparation and electromechanical testing setup in this work are identical to those in Botero-Sanchez et al. [17] For clarity, we have reproduced the descriptions here, along with the methods specific to the present study.

4.1 | Sample Preparation

Eutectic gallium-indium (EGaIn) alloy was prepared by mixing 75.5 wt.% Ga and 24.5 wt.% In and heating at 200 °C on a hot plate overnight. Gallium (Ga, 99.99%) and indium (In, 99.99%) were purchased from Rotometals, USA. Dragon Skin 10, parts A and B were purchased from Smooth-On. Polished (Mirror-Like Multipurpose) 110 copper in 24 and 28 gauge were purchased from McMaster-Carr.

To fabricate the specimens, a film of Dragon Skin 10 was first draw-coated onto PET using a custom-made drawbar with 0.5 or 1.0 mm gap height, and let cure overnight at room temperature. Next, we cut PET (polyethylene terepthalate) film into a mold with the desired trace geometry (length, width), using a CO_2 laser (VLS 3.50, Universal Laser Systems) for the straining samples. A UV laser (LPKF Protolaser U4) with higher spatial resolution laser was used for the static samples. The PET mold was placed on the silicone, with the PET thickness (0.076, 0.127, 0.254 mm) dictating the final height of the liquid metal trace. For the strain samples, square pieces of plain-weave fabric were impregnated with silicone and laid in place over the PET mold. Next, another layer of silicone was poured over the mold and fabrics, and let cure overnight. The total thickness of the sample is approximately 2 mm. The samples were then cut into a dogbone shape using the CO_2 laser. The PET mold was manually removed, leaving a rectangular channel. Finally, EGaIn was injected into the channel using a syringe with a flat-tipped needle, and both ends were plugged with 24 gauge copper wire to serve as electrodes to connect to the four-point probe multimeter (BK Precision 5492B).

4.2 | Sample Preparation of Non-EGaIn Traces

Gallium was melted in an oven at 50°C overnight, then injected into the silicone channel with a syringe. Gallium is normally solid at room temperature but has supercooling properties, allowing the encapsulated gallium traces to stay liquid at room temperature. In one specimen, the trace solidified during the strain cycle, and the trial was discarded. Traces of serpentine copper wire were made by winding 28 gauge copper wire around a fixture (detailed in Figure S13).

4.3 | Electromechanical Characterization

For electromechanical testing, the specimens were subjected to uniaxial tensile loading at 15 mm min^{-1} using a customized tensile stage controlled by an Arduino Uno. Each end of the specimen was fixed with four pins through the fabric and silicone layers (Figure 1a). The dynamic and static resistance measurements were acquired using a four-point probe method using a multimeter (BK Precision 5492B). The resistance and strain values were recorded using MATLAB R2021a.

4.4 | Analysis

Analysis was carried out using MATLAB R2023b. For the static measurements, we processed the data with the median value, as this is less sensitive to outliers than the average value. We used the *polyfit()* function to calculate linear fitsorc based on least squares. In our plots and analysis, we sampled the strain data at each integer percent strain (801 points for 400% strain). We plotted the whole strain cycle (stretching and releasing), with shaded error bars [37] on only the stretching half-cycle for clarity. For compiling prior results, we used WebPlotDigitizer to extract numerical data from plot images [38] and ran a smoothing average to reduce experimental noise in the data. We extracted values from the fitted curve of the data in Boley et al. [19]

Acknowledgments

S.J.W. was supported by the NASA NSTGRO Fellowship (80NSSC22K1188). R.K.-B. was supported by the National Science Foundation under IIS-1954591.

Conflicts of Interest

The authors declare no conflicts of interest.

Data Availability Statement

The data that support the findings of this study are available upon reasonable request from the corresponding author.

References

1. Y. G. Park, G. Y. Lee, J. Jang, S. M. Yun, E. Kim, and J. U. Park, "Liquid Metal-Based Soft Electronics for Wearable Healthcare," *Advanced Healthcare Materials* 10, no. 17 (2021): 2002280, https://onlinelibrary.wiley.com/doi/abs/10.1002/adhm.202002280.

2. S. Chen, S. Fan, H. Chan, et al., "Liquid Metal Functionalization Innovations in Wearables and Soft Robotics for Smart Healthcare Applications," *Advanced Functional Materials* (2023): 2309989, https://onlinelibrary.wiley.com/doi/abs/10.1002/adfm.202309989.

3. R. Guo, X. Wang, H. Chang, et al., "Ni-GaIn Amalgams Enabled Rapid and Customizable Fabrication of Wearable and Wireless Healthcare Electronics," *Advanced Engineering Materials* 20 (2018): 1–9.

4. M. Park, T. Park, S. J. Yoon, S. H. Koo, and Y. L. Park, "Stretchable Glove for Accurate and Robust Hand Pose Reconstruction Based on Comprehensive Motion Data," *Nature Communications* 15 (2024): no. 5821.

5. S. Chen, H. Z. Wang, T. Y. Liu, and J. Liu, "Liquid Metal Smart Materials Toward Soft Robotics," *Advanced Intelligent Systems* 5, no. 8 (2023): 2200375, https://onlinelibrary.wiley.com/doi/abs/10.1002/aisy.202200375.

6. J. Ye, Y. C. Yao, J. Y. Gao, et al., "LM-Jelly: Liquid Metal Enabled Biomimetic Robotic Jellyfish," *Soft Robotics* 9, no. 6 (2022): 1098–1107, https://doi.org/10.1089/soro.2021.0055.

7. Y. Lin, J. Genzer, and M. D. Dickey, "Attributes, Fabrication, and Applications of Gallium-Based Liquid Metal Particles," *Advanced Science* (2020): 7, 2000192, https://doi.org/10.1002/advs.202000192.

8. N. Kazem, T. Hellebrekers, and C. Majidi, "Soft Multifunctional Composites and Emulsions with Liquid Metals," *Advanced Materials* (2017): 29, 1605985, https://doi.org/10.1002/adma.201605985.

9. M. D. Dickey, "Emerging Applications of Liquid Metals Featuring Surface Oxides," *ACS Applied Materials & Interfaces* 6, no. 21 (2014): 18369–18379, https://doi.org/10.1021/am5043017.

10. S. Eristoff, A. M. Nasab, X. Huang, and R. Kramer-Bottiglio, "Liquid Metal + x: A Review of Multiphase Composites Containing Liquid Metal and Other (x) Fillers," *Advanced Functional Materials*, 34, (2024): 2309529, https://onlinelibrary.wiley.com/doi/abs/10.1002/adfm.202309529.

11. E. J. Markvicka, M. D. Bartlett, X. Huang, and C. Majidi, "An Autonomously Electrically Self-Healing Liquid Metal-Elastomer Composite for Robust Soft-Matter Robotics and Electronics," *Nature Materials* 17 (2018): 618–624, https://doi.org/10.1038/s41563-018-0084-7.

12. S. Liu, D. S. Shah, and R. Kramer-Bottiglio, "Highly Stretchable Multilayer Electronic Circuits Using Biphasic Gallium-Indium," *Nature Materials* 20 (2021): 851–858, https://doi.org/10.1038/s41563-021-00921-8.

13. S. Woodman, D. Shah, M. Landesberg, A. Agrawala, and R. Kramer-Bottiglio, "Stretchable Arduinos embedded in soft robots," *Science Robotics* 9, (2024): eadn6844, https://www.science.org/doi/10.1126/scirobotics.adn6844.

14. K. B. Ozutemiz, J. Wissman, O. B. Ozdoganlar, and C. Majidi, "EGaIn–Metal Interfacing for Liquid Metal Circuitry and Microelectronics Integration," *Advanced Materials Interfaces* 5, no. 10 (2018): 1701596, https://onlinelibrary.wiley.com/doi/abs/10.1002/admi.201701596.

15. D. G. Marques, P. A. Lopes, A. T. D. Almeida, C. Majidi, and M. Tavakoli, "Reliable Interfaces for EGaIn Multi-Layer Stretchable Circuits and Microelectronics," *Lab on a Chip* 19, no. 5 (2019): 897–906, https://pubs.rsc.org/en/content/articlelanding/2019/lc/c8lc01093e.

16. P. A. Lopes, D. F. Fernandes, A. F. Silva, et al., "Bi-Phasic Ag–In–Ga-Embedded Elastomer Inks for Digitally Printed, Ultra-Stretchable, Multilayer Electronics," *ACS Applied Materials & Interfaces* 13, no. 12 (2021): 1452–14561, https://doi.org/10.1021/acsami.0c22206.

17. L. Sanchez-Botero, D. S. Shah, and R. Kramer-Bottiglio, "Are Liquid Metals Bulk Conductors?" *Advanced Materials* 34, no. 26 (2022): 2109427, https://onlinelibrary.wiley.com/doi/abs/10.1002/adma.202109427.

18. Y. L. Park, B. R. Chen, and R. J. Wood, "Design and Fabrication of Soft Artificial Skin Using Embedded Microchannels and Liquid Conductors," *IEEE Sensors Journal* 12, no. 8 (2012): 2711–2718.

19. J. W. Boley, E. L. White, G. T. C. Chiu, and R. K. Kramer, "Direct Writing of Gallium-Indium Alloy for Stretchable Electronics," *Advanced Functional Materials* 24, no. 23 (2014): 3501–3507, https://onlinelibrary.wiley.com/doi/abs/10.1002/adfm.201303220.

20. C. Pan, K. Kumar, J. Li, E. J. Markvicka, P. R. Herman, and C. Majidi, "Visually Imperceptible Liquid-Metal Circuits for Transparent, Stretchable Electronics with Direct Laser Writing," *Advanced Materials* 30, no. 12 (2018): 1706937, https://onlinelibrary.wiley.com/doi/abs/10.1002/adma.201706937.

21. M. J. Ford, C. P. Ambulo, T. A. Kent, et al., "A Multifunctional Shape-Morphing Elastomer with Liquid Metal Inclusions," *Proceedings of the National Academy of Sciences* 116, no. 43 (2019): 21438–21444, https://www.pnas.org/doi/abs/10.1073/pnas.1911021116.

22. U. Daalkhaijav, O. D. Yirmibesoglu, S. Walker, and Y. Mengüç, "Rheological Modification of Liquid Metal for Additive Manufacturing of Stretchable Electronics," *Advanced Materials Technologies* 3, no. 4 (2018): 1700351, https://onlinelibrary.wiley.com/doi/abs/10.1002/admt.201700351.

23. A. B. M. T. Haque, R. Tutika, M. Gao, et al., "Conductive Liquid Metal Elastomer Thin Films with Multifunctional Electro-Mechanical Properties," *Multifunctional Materials* 3, no. 4 (2020): 044001, https://dx.doi.org/10.1088/2399-7532/abbc66.

24. H. Chang, P. Zhang, R. Guo, et al., "Recoverable Liquid Metal Paste with Reversible Rheological Characteristic for Electronics Printing," *ACS Applied Materials & Interfaces* 12, no. 12 (2020): 14125–14135, https://doi.org/10.1021/acsami.9b20430.

25. R. A. Bilodeau, A. M. Nasab, D. S. Shah, and R. Kramer-Bottiglio, "Uniform Conductivity in Stretchable Silicones: Via Multiphase Inclusions," *Soft Matter* 16 (2020): 5827–5839.

26. S. Zhu, J. H. So, R. Mays, et al., "Ultrastretchable Fibers with Metallic Conductivity Using a Liquid Metal Alloy Core," *Advanced Functional Materials* 23, no. 18 (2013): 2308–2314, https://onlinelibrary.wiley.com/doi/abs/10.1002/adfm.201202405.

27. C. S. M. Pouillet, *Éléments de Physique Expérimentale et de Météorologie* (Paris: Béchet, 1837).

28. N. Zolfaghari, P. Khandagale, M. J. Ford, K. Dayal, and C. Majidi, "Network Topologies Dictate Electromechanical Coupling in Liquid Metal-Elastomer Composites," *Soft Matter* 16 (2020): 8818–8825.

29. W. Monnens, B. Zhang, Z. Zhou, et al., "Scalable Electrodeposition of Liquid Metal from an Acetonitrile-Based Electrolyte for Highly Integrated Stretchable Electronics," *Advanced Materials* 35, no. 51 (2023): 2305967, https://onlinelibrary.wiley.com/doi/10.1002/adma.202305967.

30. Z. J. Farrell and C. Tabor, "Control of Gallium Oxide Growth on Liquid Metal Eutectic Gallium/Indium Nanoparticles via Thiolation," *Langmuir* 34, no. 1 (2018): 234–240, https://doi.org/10.1021/acs.langmuir.7b03384.

31. A. Zheng and A. Casari, "Feature Engineering for Machine Learning: Principles and Techniques for Data Scientists," O'Reilly Media, Sebastopol, CA (2018).

32. G. Reeves and H. Harrison, "Obtaining the Specific Contact Resistance from Transmission Line Model Measurements," *IEEE Electron Device Letters* 3, no. 5 (1982): 111–113.

33. D. Zrnic and D. Swatik, "On the Resistivity and Surface Tension of the Eutectic Alloy of Gallium and Indium," *Journal of the Less Common Metals* 18, no. 1 (1969): 67–68, https://www.sciencedirect.com/science/article/pii/0022508869901210.

34. M. Pokorny and H. U. Astrom, "Temperature Dependence of the Electrical Resistivity of Liquid Gallium Between its Freezing Point (29.75 degrees C) and 752 degrees C," *Journal of Physics F: Metal Physics* 6, no. 4 (1976): 559, https://dx.doi.org/10.1088/0305-4608/6/4/015.

35. J. G. G. G. Ginter and R. Kleim, "The Electrical Resistivity of Liquid Bismuth, Gallium and Bismuth-Gallium Alloys," *Philosophical Magazine B* 54, no. 6 (1986): 543–552, https://doi.org/10.1080/13642818608236869.

36. L. X. Yang and A. Ettemeyer, "Strain Measurement by Three-Dimensional Electronic Speckle Pattern Interferometry: Potentials, Limitations, and Applications," *Optical Engineering* 42, no. 5 (2003): 1257–1266, https://doi.org/10.1117/1.1566781.

37. R. Campbell, "raacampbell/shadedErrorBar," (2024), https://github.com/raacampbell/shadedErrorBar.

38. A. Rohatgi, "WebPlotDigitizer," (2024), https://automeris.io/WebPlotDigitizer.html.

Supporting Information

Additional supporting information can be found online in the Supporting Information section.

Supporting File: admt70850-sup-0001-SuppMat.pdf.